



Plasmon-enhanced perovskite solar cells using ultra-thin LiF spacer isolating AgAl and Au composite nanoparticles from metal electrode

Weijia Xie^a, Jianping Zhou^b, Sumei Huang^a, Wei Ou-Yang^a, Wenhui Xie^{a,*}, Zhuo Sun^a, Xiaohong Chen^{a,**}

^a Engineering Research Center for Nanophotonics and Advanced Instrument, Ministry of Education, School of Physics and Materials Science, East China Normal University, Shanghai, 200062, China

^b School of Automation Engineering, Shanghai University of Electric Power, Shanghai, 200090, China

ARTICLE INFO

Keywords:

Perovskite solar cells
AgAl
Au
Plasmon resonance
Work function

ABSTRACT

Plasmon enhanced perovskite solar cells (PSCs) incorporated with AgAl and Au composite nanoparticles (NPs) isolating from AgAl metal electrode with ultra-thin LiF spacer were investigated. PSCs with AgAl-Au composite NPs got 17.02% of the power conversion efficiency (PCE), which is 11.10% higher than PCE (15.32%) of the control PSC with only AgAl electrode. Furthermore, the hysteresis effect of PSCs with LiF modified AgAl and Au composite NPs can be neglected compared to the control cells without NPs and LiF spacer. In the meanwhile, carrier transport and collection probabilities of PSCs with AgAl and Au composite NPs were increased to 96.86% from 89.51% in control cells, indicating the improved electron transport and extraction ability. The enhanced PCEs of PSCs with AgAl(3 nm)/Au(2 nm)/LiF(1 nm) are attributed to the improved light absorption of perovskite layer and the reduced contact barrier at metal electrode, which can be supported with its enhanced photon-to-electron conversion efficiency (Δ IPCE) and the disappeared negative capacitive behavior. Furthermore, the obviously reduced work function values of AgAl-Au composite NPs and AgAl metal electrode after LiF modification were observed with ultraviolet photoelectron spectroscopy spectra. Our results indicate that thermally evaporating a ultra-thin LiF spacer can well inhibit the energy dissipation of plasmon effects of AgAl-Au composite NPs and reduce the contact barrier between PCBM and AgAl metal electrode, which is an efficient strategy to achieve efficient plasmon-enhanced perovskite solar cells.

1. Introduction

Perovskite solar cells (PSCs) have attracted great attention due to its promising advantages such as ease of fabrication, low-cost and high efficiency [1–6]. The power conversion efficiency (PCE) of PSCs has rapidly increased and broken through 20% in 2015 from 3% in 2009 [2,4]. Eventually, the certified PCE of PSCs was further promoted to 22.7%, which is approaching PCEs of commercial poly/monocrystalline silicon solar cells [5,6].

PSCs are usually divided into mesoporous structure and planar structure perovskite solar cells according to the different transmission layer structure. In the typical mesoporous PSCs, a mesoporous TiO₂ scaffold to support the perovskite layer can boost electron transport and extract from perovskite layer to the electron transport layer, which can tolerate more thickness (typical 400–500 nm) of perovskite layer to obtain high efficient PSCs [3]. Furthermore, the mesoporous scaffolds usually have light scatter function, which can further increase light

absorption of perovskite layer [7]. While planar perovskite solar cells usually have less thickness and typical thickness of 200–350 nm for high efficient planar PSCs because the thicker perovskite layer can inhibit carriers transport and extraction efficiency [8]. Therefore, planar PSCs compared to mesoporous structure PSCs show less efficiency because the thinner perovskite active layer cannot fully absorb sunlight [9,10]. However, planar perovskite solar cells compared to mesoporous PSCs are expected to have more unique advantages such as more simple fabrication, lower cost and more easily flexibility, which boost scientists to seek more efficient planar PSCs [11,12].

Noble metal (Au and Ag) nanoparticles and nanostructures have demonstrated an effective method to improve the light trapping capability of solar cells because of its localized surface plasmon resonance effects (LSPRs), which have been successfully used to improve PCEs of organic solar cells [13,14], dye-sensitized solar cells [15,16] and perovskite solar cells [10,17]. The metal nanoparticles (NPs) may usually be embedded into the photoactive layer, and/or carrier transport layer

* Corresponding author.

** Corresponding author.

E-mail addresses: whxie@phy.ecnu.edu.cn (W. Xie), xhchen@phy.ecnu.edu.cn (X. Chen).

to improve light absorption of the photoactive layer [18–21]. The metal NPs embedded in the photoactive layer need to be covered with the insulator layer to avoid carrier recombination at the surface of metal NPs. Metal NPs are preferred to be embedded into the carrier transport layer, which can isolate metal NPs from the photoactive layer. Furthermore, the uncovered metal nanoparticles embedded into the carrier transport layer and modification layer can also reduce serial resistance of cells due to its high conductivity [22–24]. Therefore, the enhanced efficiency of perovskite and polymer solar cells embedded metal NPs into carrier transport layer have been extensively reported, which are primarily attributed to the increased absorption of the photoactive layer and the improved carrier transport and extraction ability due to the reduced serial resistance [21,25].

The plasmonic effects such as resonance light wavelength and intensity of metal NPs can be flexibly adjusted by the type of metal used, the morphologies, sizes, arrangements of NPs and the surrounding medium [20,22,26]. Using Ag and Au dual NPs can greatly extend the resonance wavelength range, which may realize the whole light absorption enhancement in the visible and near-IR wavelengths [20]. Lu et al. reported a 20% PCE enhancement of polymer solar cells, where an Ag and Au mixture NPs were incorporated into hole-transport layer, resulting in the obviously increased light absorption of perovskite photoactive layer and the improved carrier transport and extraction [27]. Fu et al. incorporated Au@Ag core-shell nanocuboids into electron transport layer for meso-superstructure PSCs, leading to a synergistic plasmonic enhancement in PSCs. The excellent plasmonic properties of Au@Ag nanocuboids yielded a champion PCE of 18.31% for the hybrid PSCs, corresponding to 20.8% enhancement compared with the pristine cells [23]. The metal NPs or metal nanostructures incorporated into the rear side compared to the front side of the photoactive layer usually have some advantages such as inhibiting the destructive interference due to the Fano resonance effect and weakening light loss caused by the self-absorption of metal NPs [28,29]. In the meanwhile, metal NPs or metal nanostructures located at the rear side of cells may easily be fabricated by a simple thermal evaporation technique, and its plasmon effects including the resonance wavelength ranges and intensity can be flexibly adjusted by changing nominal thicknesses of metal, types of metal and surrounding medium [13,26,30,31]. Yao et al. evaporated Ag and Au NPs in the WO_3 anode buffer layer in inverted polymer solar cells, which greatly improved PCE due to widening the resonance wavelength range [30]. However, metal NPs inserted into the WO_3 layer can induce the shift of both work function and valence band of contact interface between metal NPs and WO_3 layer, which would produce another energy barrier at the location of metal NPs when carriers transport from the photoactive layer to metal electrode. The 5-nm thick WO_3 isolating layer between metal NPs and Ag electrode is expected to reduce carrier tunnel probability from metal NPs to Ag electrode, which would partly offset the advantage of reduced serial resistance due to metal high conductivity [13,30,31]. In this paper, AgAl-Au composite NPs combined with ultra-thin LiF spacer were firstly modified onto AgAl metal electrode of perovskite solar cells by thermally evaporation method. LiF as a spacer have been successfully applied to plasmon based polymer solar cells in our previous report [26]. The perovskite layer have severer roughness compared to polymer photoactive layer due to the large size perovskite grains. However, the plasmon effects of AgAl-Au composite NPs evaporated onto rough surface of perovskite/PCBM substrates can still be retained by a ultra-thin LiF spacer of only 1 nm thickness, which obviously improve the light absorption of perovskite layer. Furthermore, the LiF spacer has modification function and can obviously reduce work function of AgAl electrode, AgAl-Au composite NPs, which boost electrons of PCBM layer easily cross the composite metal NPs and LiF spacer and further transport to AgAl metal electrode because of the reduced contact barrier between AgAl electrode and AgAl-Au composite NPs.

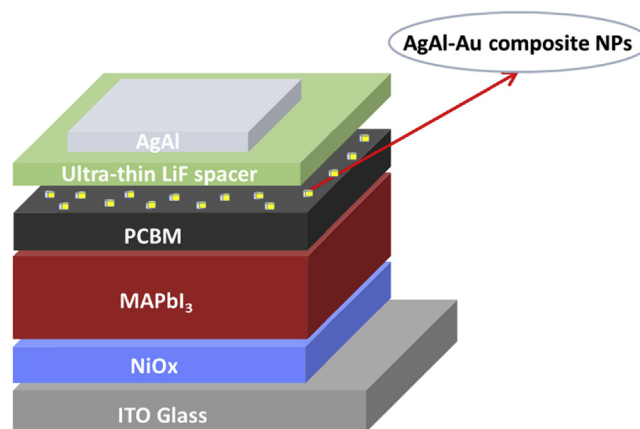


Fig. 1. Schematic graph of PSCs with AgAl-Au composite NPs modified electrode.

2. Experimental section

PSCs with a structure of Glass/ITO/ NiO_x /MAPbI₃/PCBM/AgAl-Au composite NPs/LiF/AgAl were fabricated, as shown schematically in Fig. 1.

The pre-patterned indium tin oxide (ITO)/glass substrates with a sheet resistance of 10 Ω /sq were cleaned by ultra-sonication sequentially in detergent, de-ionized water, acetone and isopropanol for 20 min. After being dried in the oven, ITO coated glass substrates were treated with ultraviolet ozone for 15 min. NiO precursor solution was then spin-coated at 4500 rpm for 45 s to form a 20-nm thick film, followed by annealing at 275 $^\circ\text{C}$ for 45 min in air. In a typical synthesis, the nickel acetate tetrahydrate ($\text{Ni}(\text{CH}_3\text{COO})_2(4\text{H}_2\text{O})$) was dissolved in 2-methoxyethanol ($\text{C}_3\text{H}_8\text{O}_2$) with monoethanolamine ($\text{NH}_2\text{CH}_2\text{CH}_2\text{OH}$) (MEA) (Sigma-Aldrich) (0.1 mol/L). The mole ratio of Ni^{2+} : MEA was maintained at 1:1 in solution. Then the solution was stirred in a glass vial under air at 70 $^\circ\text{C}$ for 4 h. The solution appeared homogeneous and deep green after approximately 40 min [32]. After stirring, the solution was stored in a refrigerator at 5 $^\circ\text{C}$. Then NiO_x films were allowed to cool down before being transferred to a nitrogen-filled glovebox for further processing. The perovskite precursor solution was prepared by dissolving 1 M methyl ammonium iodide (MAI, 1-Material Inc.) and 1 M lead (II) iodide (PbI_2 , 99.9%, Aladdin Reagents) in a mixture of dimethyl sulphoxide (DMSO, AR 99% GC, Aladdin Reagents) and γ -Butyrolactone (GBL, AR 99% GC, Aladdin Reagents) (7:3 v/v). After stirring overnight, the solution was ready for use. The $\text{CH}_3\text{NH}_3\text{PbI}_3$ (MAPbI₃) film was spin-coated on the surface of NiO_x hole-transport layer by a consecutive two-step spin-coating process at 1500 rpm for 15 s and 4000 rpm for 60 s, respectively. During the second spin-coating step at 30 s, 0.5 ml of anhydrous chlorobenzene (Alfa Aesar) was quickly dropped onto the surface of perovskite layer, then the substrate was heated at 100 $^\circ\text{C}$ for 10 min. After being cooled down, the [6,6]-phenyl-C61-butyric acid methyl ester (PCBM) solution (10 mg/ml in chlorobenzene) was spin-coated at 1200 rpm to form a 40-nm thick film on top of the perovskite layer. Finally, a 3-nm thick AgAl, different nominal thicknesses of Au and LiF spacer, and 100-nm thick AgAl electrode were sequentially deposited by thermal evaporation with a base pressure of 3×10^{-4} Pa using a shadow mask of 0.1 cm^2 . The weight ratio (wt%) of Al to Ag in the AgAl alloy, purchased from Trillion Metals Co., Ltd. (Beijing, China), is 3 wt%. A mask with an aperture area of 0.09 cm^2 was used for the current density-voltage (J-V) characteristic measurement to avoid the edge effect.

The J-V characteristics of PSCs were measured with a Keithley 2440 SourceMeter together with a Newport solar simulator with an AM1.5G illumination of 100 mW/cm^2 calibrated with a standard silicon reference cell. The incident-photon-to-current conversion efficiencies (IPCEs) of the PSCs were measured over the wavelength range from 300

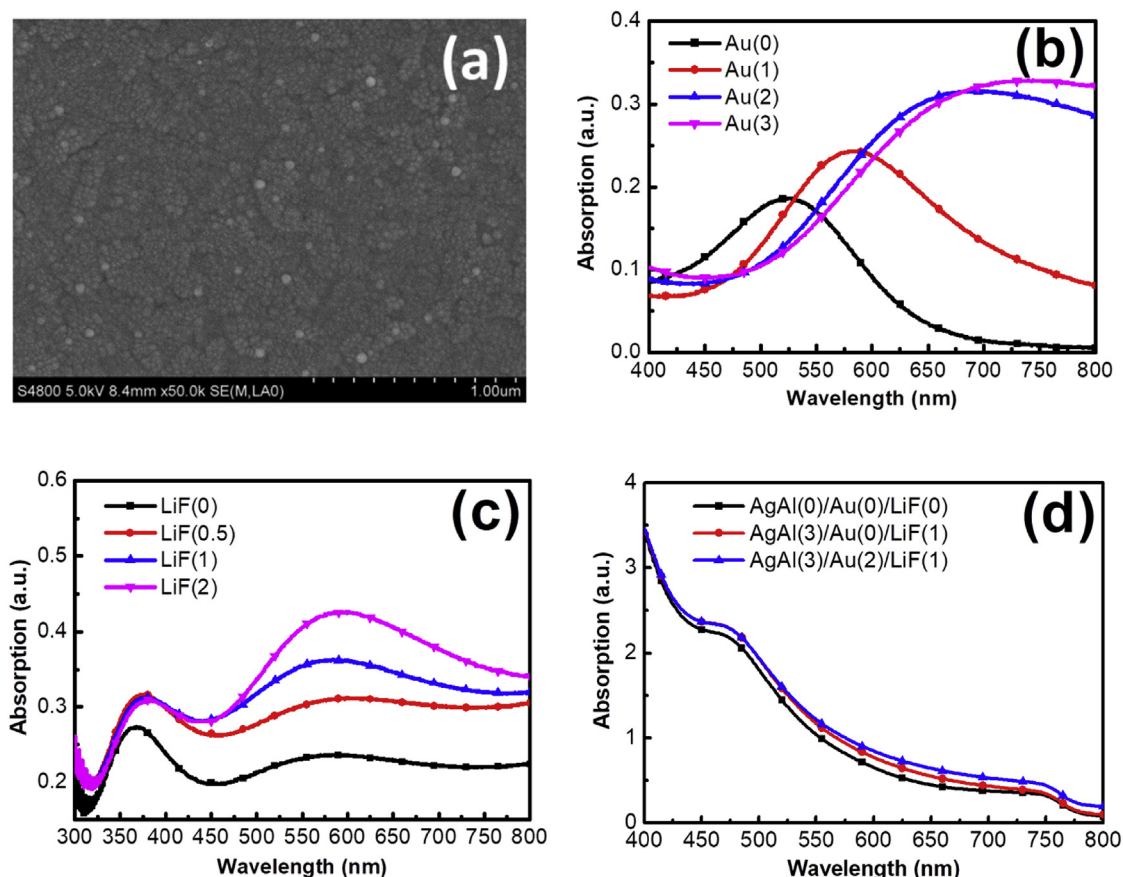


Fig. 2. (a) SEM image of AgAl(3)/Au(2) composite NPs thermally evaporated on top of the glass/ITO substrate. (b) Absorption spectra of AgAl(3)/Au(x) NPs onto glass/ITO substrate. (c) Absorption spectra of AgAl(3)/Au(2) NPs isolated from metal electrode with different thick LiF spacer, where simulating electrode structure glass/ITO/AgAl(3)/Au(2)/LiF(y)/Al(10). (d) Absorption spectra of perovskite/PCBM layer evaporated without and with AgAl/Au composite NPs and LiF spacer. The numbers in parentheses indicate the average layer thicknesses in nanometers.

to 800 nm using a Newport Optical Power Meter 2936-R controlled by TracQ Basic software, where the baseline were calibrated with a detector (model 71683 v3, Oriol Instruments). The electrochemical impedance spectra (EIS) were measured in the dark using an electrochemical workstation (Autolab PGSTAT302 N). The absorption and reflectivity spectra of samples were measured using a UV/vis spectrophotometer (Hitachi U-3900). The surface morphologies of samples were investigated by field-emission scanning electron microscopy (FESEM, Hitachi S-4800). Ultraviolet photoelectron spectroscopy (UPS) spectra were measured with a monochromatic He I light source (21.22 eV) and a VG Scienta R4000 analyzer.

3. Results and discussion

The white island-shaped composite nanoparticles of AgAl and Au were clearly formed due to the aggregation of AgAl and Au during the thermal evaporation, as shown in Fig. 2a. The sizes of most of the metal island NPs were about 20–50 nm, indicating that the relatively uniform distribution of AgAl-Au island-like NPs can be achieved by simple thermal evaporation, which can produce localized surface plasmon resonance effects in solar cells.

The plasmon effects of AgAl and Au composite NPs can be adjusted by thermally evaporating different thicknesses of Au film, as shown in Fig. 2b. The broad light absorption range of AgAl-Au composite NPs is different from the absorption of those small sized Au and Ag nanoparticles formed by the chemical synthesis [33]. The red light wavelength is obviously enhanced with increasing Au film and the surface resonance wavelength range of AgAl and Au composite NPs are widened due to their good complementarities of plasmon resonance

wavelength. However, the plasmon effects such as wavelength and resonance intensity of AgAl/Au NPs in realistic perovskite solar cells are different from that of AgAl/Au NPs in Fig. 2b, because the covered LiF isolating layer and almost adjacent AgAl electrode can change the surrounding medium of metal NPs. To simulate the plasmon effects of NPs in solar cells, the absorption spectra of AgAl and Au composite NPs simulating full cathode structures of PSCs are shown in Fig. 2c. A 10-nm thick Al electrode instead of a AgAl electrode was evaporated onto the LiF spacer in the simulated structure to avoid the surface plasmon resonance (SPR) effects of AgAl films [13]. The absorption intensity of wavelength range from 650 nm to 800 nm are obviously reduced compared to that of metal NPs from Fig. 2b, indicating that the plasmon effects of metal NPs in full structures cathode have been obviously changed. When Al was directly evaporated onto AgAl and Au composite NPs, the plasmon effects of the AgAl and Au composite NPs are almost disappeared due to the energy dissipation and inserting a 1-nm thick LiF spacer layer can well retain its plasmon resonance characteristics, indicating that this engineered cathode is an efficient way to retain the desirable plasmonic features of AgAl and Au composite NPs and lead to absorption and photocurrent enhancement in perovskite solar cells [26]. The absorption of perovskite film is obviously enhanced by the deposition of metal NPs, as shown in Fig. 2d, although this result cannot be simply interpreted as enhanced absorption by the perovskite layer. The long absorption wavelength range from 600 nm to 800 nm of perovskite film covered with AgAl and Au composite NPs compared to AgAl NPs is further increased, indicating that the widen plasmon resonance wavelength for AgAl-Au composite NPs helps to improve the whole light absorption of perovskite film [34].

To investigate the effects of incorporating plasmonic structures into

Table 1

Parameters of PSCs incorporated with different thicknesses of AgAl/Au composite NPs and LiF spacer under AM 1.5G Illumination at 100 mW/cm².

AgAl/Au/ LiF (nm)	J _{sc} (mA/cm ²)	V _{oc} (V)	FF (%)	PCE (%)	R _s (Ω)
0/0/0	19.64 ± 0.42	1.05 ± 0.01	73.5 ± 0.4	15.16 ± 0.16	66.4
3/0/1	20.04 ± 0.34	1.05 ± 0.01	75.5 ± 0.2	15.99 ± 0.11	50.6
3/1/1	20.62 ± 0.23	1.05 ± 0.01	75.6 ± 0.2	16.37 ± 0.12	46.8
3/2/1	21.29 ± 0.35	1.05 ± 0.01	75.4 ± 0.3	16.87 ± 0.15	43.5
3/3/1	20.82 ± 0.24	1.05 ± 0.01	74.3 ± 0.2	16.19 ± 0.12	55.0
3/2/0.5	20.85 ± 0.31	1.05 ± 0.01	75.0 ± 0.2	16.32 ± 0.14	49.0
3/2/2	20.17 ± 0.25	1.05 ± 0.01	75.6 ± 0.3	16.01 ± 0.11	60.8

the electrode on the PCEs of PSCs, we fabricated sets of seven types of cells. The average parameters and standard deviations of these types of cells are summarized in Table 1. Fig. 3a shows best J-V curves of PSCs with different nominal thicknesses of Au film. The optimized nominal thicknesses of AgAl and LiF spacer layers are 3 nm and 1 nm, respectively. The thicknesses of Au film are varied from 0 to 3 nm to obtain AgAl and Au composite NPs. The best J-V curves of PSCs varied with LiF thicknesses of 0.5–2 nm are also shown in Fig. 3b. Here, PSCs without LiF modified layer were chosen as the control cells to clearly show LiF functions such as reduced work function and improving contact properties, besides isolating function. While J-V curves and IPCE spectra of perovskite solar cells with and without LiF modified layer are shown in Fig. S1 and Table S1 in the Supporting Information to clearly evaluate the performance of PSCs with and without LiF modified layer. The average efficiencies of PSCs with and without LiF modified layer are respectively 15.52% and 15.16%, indicating that PSCs incorporated with LiF show slightly improved PCE compared to PSCs without LiF modified layer, but still far lower than that of PSCs incorporated with AgAl/Au nano-particles. The best PSCs with the electrode structure of AgAl(3 nm)/Au(2 nm)/LiF(1 nm)/AgAl(100 nm) got PCE = 17.02%, which is 11.10% higher than PCE (15.32%) of the control cells. The serial resistance (R_s) value of PSCs is gradually increased to 60.8 Ω from 43.5 Ω as the thickness of LiF layer is increased to 2 nm from 1 nm because the thicker LiF spacer can serve as insulators which inhibit electron extraction at the cathode [35]. The best PCE of PSCs with AgAl(3)/Au(2)/LiF(1)/AgAl(100) is attributed to the higher photocurrent and fill factor, which is possibly due to the enhanced absorption of perovskite layer and the improved electron transport and extraction efficiencies.

The plasmon enhanced effects can usually be observed by the incident photon-to-electron conversion efficiency (IPCE) spectra [13,30]. The IPCE spectra of three typical types of PSCs with and without AgAl and Au composite NPs are shown in Fig. 4a. The photocurrent of PSCs

with metal NPs is obviously enhanced compared to the control PSCs. Furthermore, the photocurrent of PSCs with AgAl and Au composite NPs compared to single AgAl NPs is obviously widened and enhanced in the light absorption range from 400 nm to 700 nm. This can be more clearly observed by plotting the enhanced Δ IPCE values as a function wavelength, where the Δ IPCE is equal to $(\text{IPCE}_{\text{plasmonic}} - \text{IPCE}_{\text{control}}) / \text{IPCE}_{\text{control}}$, as shown in Fig. 4b. The enhanced relative Δ IPCE curve roughly matches the absorption spectra profiles of AgAl-Au composite NPs/LiF/Al, indicating that plasmon effects of AgAl-Au composite NPs can greatly induce improvements in the PCEs of PSCs due to its widened and improved light absorption [24,30].

The serious hysteresis phenomena of perovskite solar cells can usually be observed when PSCs meet some typical problems such as the unbalanced charge transportation and accumulation inside the perovskite layer, the inferior grain quality of perovskite, ion migration, ferroelectricity, inferior carrier transport and collection ability, etc [4,36–39]. While superior structures of PSCs can greatly inhibit the hysteresis effect, which help to judge and improve the performance of cells [9,22]. The J-V curves of three typical types of PSCs with forward and reverse scans at a scanning rate of 0.1 V/s are shown in Fig. 5, and the detailed photovoltaic parameters are summarized in Table 2. The PCEs of PSCs with AgAl(3)/Au(2)/LiF(1) for reverse and forward scans are respectively 16.76% and 16.64%, which yielded a difference of 0.7% in PCE values, indicating the neglected hysteresis effect. Considering the similar procedures for NiO_x, perovskite and PCBM layers, the neglected hysteresis effect of PSCs with AgAl and Au composite NPs would be ascribed to less carrier accumulation due to the improved carrier transport and extraction ability.

To demonstrate the improved carrier transport and exaction ability for complex electrode structure of AgAl(3)/Au(2)/LiF(1)/AgAl(100), the J_{ph} - V_{eff} curves of three typical types of PSCs were measured, as shown in Fig. 6a. J_{ph} is defined as J_{ph} = J_L - J_D, where J_L and J_D are the current densities under illumination and in the dark, respectively. V_{eff} is determined as V_{eff} = V₀ - V_a, where V₀ is the voltage at which J_{ph} = 0 and V_a is the applied bias voltage. Generally, the saturated photocurrent (J_{sat}) is correlated with the maximum exciton generation rate, exciton dissociation probability, and carrier transport and collection probabilities [P(E,T)] in the high V_{eff} range. The P(E,T) at any effective voltage can be directly obtained from the ratio of J_{ph}/J_{sat} [13,27,40]. The P(E,T) of PSCs with AgAl-Au composite NPs was increased to 96.86% from 89.51% in control cells, indicating that LiF modified AgAl-Au NPs complex electrode can efficiently improve electron transporting and collection abilities of cells.

Impedance spectroscopy is a powerful technique to derive insights into the interfacial properties and the charge carrier dynamics of PSCs [41,42]. The different interface barrier between PCBM and AgAl

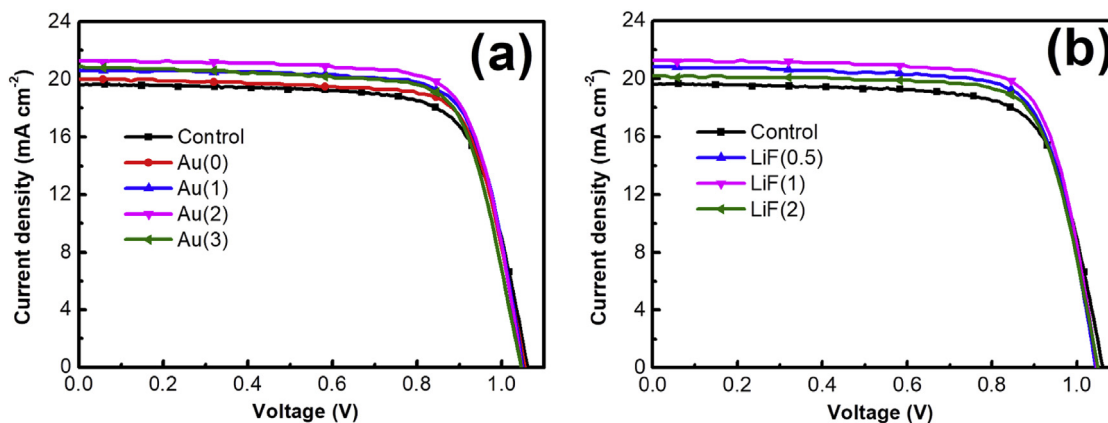


Fig. 3. J-V curves of PSCs with different nominal thicknesses of AgAl and Au composite NPs. (a) Different Au layer thicknesses with electrode structure of AgAl(3)/Au(x)/LiF(1)/AgAl(100) and (b) Different LiF spacer thicknesses with electrode structure of AgAl(3)/Au(2)/LiF(y)/AgAl(100). The control PSCs presented was only 100-nm thick AgAl electrode and without LiF modified layer. The numbers in parentheses indicate the average layer thicknesses in nanometers.

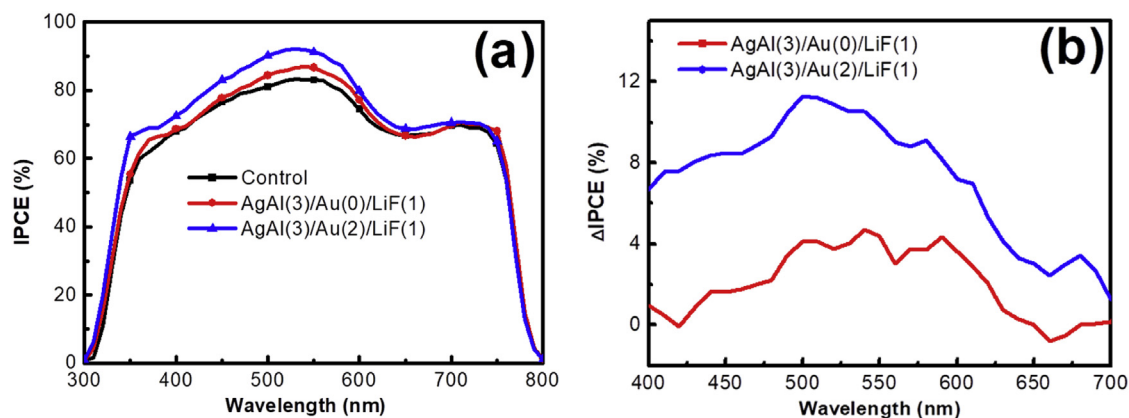


Fig. 4. (a) IPCE spectra of three typical types of PSCs with electrode structure AgAl(3)/Au(x)/LiF(1)/AgAl(100). (b) Enhanced Δ IPCE values were normalized with respect to that of the control cell with only 100-nm thick AgAl electrode and without LiF modified layer. The numbers in parentheses indicate the average layer thicknesses in nanometers.

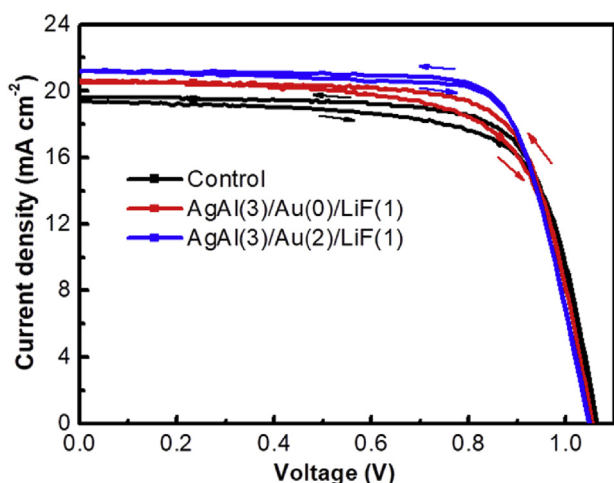


Fig. 5. The J-V curves of three typical types of PSCs with forward and reverse scans at a scanning rate of 0.1 V/s.

Table 2

Parameters of three typical types of PSCs with forward and reverse scans under 1.5G illumination at 100 mW/cm².

AgAl/Au/LiF (nm)	Scan direction	J _{sc} (mA/cm ²)	V _{oc} (V)	FF (%)	PCE (%)
000	Reverse	19.64	1.05	73.5	15.21
	Forward	19.37	1.05	70.9	14.48
301	Reverse	20.60	1.05	74.1	16.03
	Forward	20.61	1.05	68.8	14.97
321	Reverse	21.20	1.05	75.3	16.76
	Forward	21.19	1.05	74.8	16.64

electrode is expected to affect carrier accumulation and transportation, resulting in differences in the device capacitance. Fig. 6b shows the impedance spectra of three types of PSCs measured in a frequency range of 0.1–10⁶ Hz at forward bias voltage of 0.9 V under dark condition. The impedance plots of the control cells exhibits an arc in the fourth quadrant at the low frequency range, indicating the negative capacitance exists in PSCs. The negative capacitive behavior of cells with LiF modified AgAl-Au composite NPs is disappeared, indicating that the electron carrier accumulation of PSCs is greatly reduced due to the improved contact properties for AgAl(3)/Au(2)/LiF(1)/AgAl(100) electrode, which supports the conclusion of the reduced carrier accumulation at the interface drawn from its neglected hysteresis effect.

To further illustrate the reduced contact barrier for LiF modified AgAl-Au composite NPs, the values of work function for AgAl and Au

composite NPs with and without LiF modification are shown in Fig. 7a. The work function values of AgAl-Au composite NPs and pure AgAl NPs are respectively 4.39 eV and 4.43 eV, which are larger than the Fermi energy (E_F 4.14 eV) of PCBM layer. However, the work function values of single AgAl NPs and AgAl-Au composite NPs modified with LiF spacer layer was greatly decreased and obtained 4.03 eV and 4.18 eV, respectively. Considering metal electrode is AgAl, this means that LiF as isolating layer between AgAl-Au composite NPs and AgAl metal electrode can also reduce the work function of AgAl electrode, which can further decrease the contact barrier and help to improve electron transport and extraction abilities. The schematic graph of energy level alignment is shown in Fig. 7b. The reduced work function values for AgAl-Au composite NPs and AgAl metal electrode due to the effect of LiF modification can form the synergism effect to reduce the contact barrier of metal electrode and improve carrier transport and collection ability, which partly contribute to the enhanced PCE of PSCs.

4. Conclusions

In conclusion, the plasmonic performance of PSCs with AgAl-Au composite NPs modified with LiF spacer by thermal evaporation method were investigated. The optimal PSCs with the structure of glass/ITO/NiO_x/perovskite/PCBM/AgAl(3)/Au(2)/LiF(1)/AgAl(100) can reach 17.02% of PCE, which is obviously higher than PCE (15.32%) of the control cells. The absorption spectra of AgAl-Au composite NPs reveal a prominent increase in light absorption by the plasmon resonance. The higher photocurrent and fill factors contribute to the enhanced PCE of PSCs, which are primarily attributed to the enhanced light absorption of perovskite layer and the improved electron transport and extraction abilities. The obviously reduced work function of AgAl-Au composite NPs and AgAl electrode due to the effect of LiF modification further support the improved contact properties between PCBM and AgAl electrode. The strategy of AgAl-Au composite NPs isolated from AgAl metal electrode with ultra-thin LiF spacer is an effective method to obtain high efficiency perovskite solar cells because of its composite functions for inhibiting energy dissipation of plasmon effects and reducing contact barrier of metal electrode.

Acknowledgements

This work was supported by Natural Science Foundation of Shanghai (Nos. 18ZR1411000 and 18ZR1411900) and National Natural Science Foundation of China (No. 61275038).

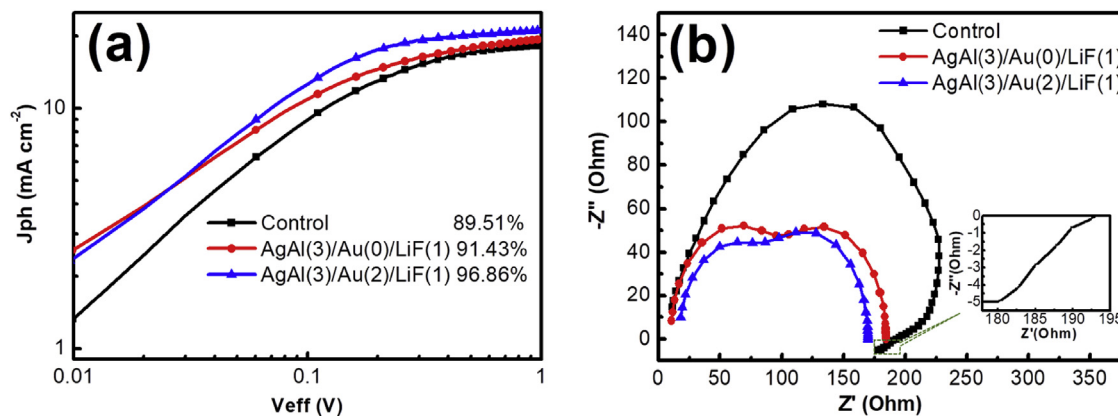


Fig. 6. (a) Plots of J_{ph} versus V_{eff} for three typical types of cells. (b) The impedance spectra of three types of PSCs measured with the frequency range of 0.1–10⁶ Hz at forward bias voltage of 0.9 V in dark condition.

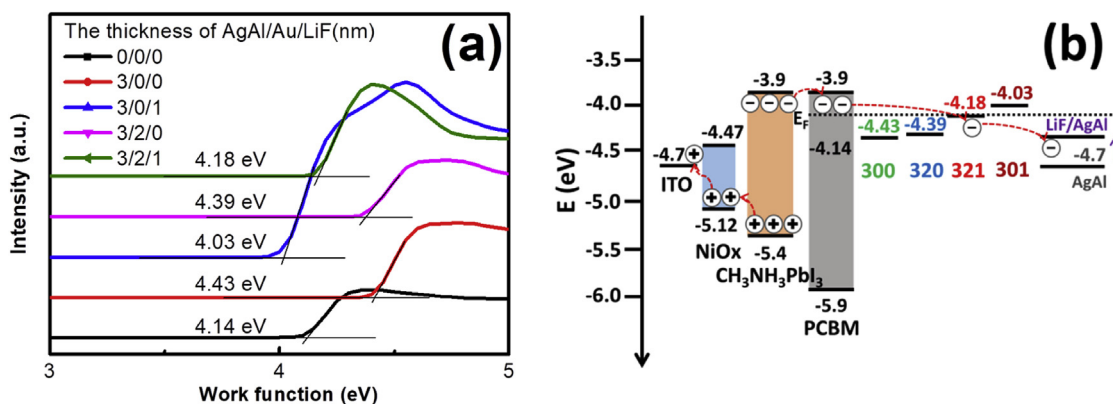


Fig. 7. (a) Work function values for AgAl and AgAl-Au composite NPs with and without LiF modification measured with UPS spectra. (b) Schematic energy levels of each layer in perovskite solar cell.

Appendix A. Supplementary data

Supplementary data related to this article can be found at <http://dx.doi.org/10.1016/j.orgel.2018.05.020>.

References

- G. Xing, N. Mathews, S. Sun, S.S. Lim, Y.M. Lam, M. Grätzel, S. Mhaisalkar, T.C. Sum, Long-range balanced electron- and hole-transport lengths in organic-inorganic CH₃NH₃PbI₃, *Science* 342 (6156) (2013) 344–347.
- A. Kojima, K. Teshima, Y. Shirai, T. Miyasaka, Organometal halide perovskites as visible-light sensitizers for photovoltaic cells, *J. Am. Chem. Soc.* 131 (17) (2009) 6050–6051.
- H.S. Kim, C.R. Lee, J.H. Im, K.B. Lee, T. Moehl, A. Marchioro, S.J. Moon, R. Humphry-Baker, J.H. Yum, J.E. Moser, M. Grätzel, N.G. Park, Lead iodide perovskite sensitized all-solid-state submicron thin film mesoscopic solar cell with efficiency exceeding 9%, *Sci. Rep.* 2 (8) (2012) 591.
- N.J. Jeon, J.H. Noh, W.S. Yang, Y.C. Kim, S. Ryu, J. Seo, S.I. Seok, Compositional engineering of perovskite materials for high-performance solar cells, *Nature* 517 (7535) (2015) 476–480.
- M.K. Nazeeruddin, In retrospect: twenty-five years of low-cost solar cells, *Nature* 538 (7626) (2016) 463–464.
- H. Tang, S. He, C. Peng, A short progress report on high-efficiency perovskite solar cells, *Nanoscale research letters* 12 (1) (2017) 4101–4108.
- X. Hou, L. Pan, S. Huang, O.-Y. Wei, X. Chen, Enhanced efficiency and stability of perovskite solar cells using porous hierarchical TiO₂ nanostructures of scattered distribution as scaffold, *Electrochim. Acta* 236 (2017) 351–358.
- Z. Xiao, C. Bi, Y. Shao, Q. Dong, Q. Wang, Y. Yuan, C. Wang, Y. Gao, J. Huang, Efficient, high yield perovskite photovoltaic devices grown by interdiffusion of solution-processed precursor stacking layers, *Energy Environ. Sci.* 7 (8) (2014) 2619–2623.
- R. Wu, B. Yang, C. Zhang, Y. Huang, Y. Cui, P. Liu, C. Zhou, Y. Hao, Y. Gao, J. Yang, Prominent efficiency enhancement in perovskite solar cells employing silica-coated gold nanorods, *J. Phys. Chem. C* 120 (13) (2016) 6996–7004.
- D.S. Lee, W. Kim, B.G. Cha, J. Kwon, S.J. Kim, M. Kim, J. Kim, D.H. Wang, J.H. Park, Self-positioning of Au NPs in perovskite solar cells: optical and electrical contribution, *ACS Appl. Mater. Interfaces* 8 (1) (2016) 449–454.
- H. Luo, X. Lin, X. Hou, L. Pan, S. Huang, X. Chen, Efficient and air-stable planar perovskite solar cells formed on graphene-oxide-modified PEDOT: PSS hole transport layer, *Nano-micro Lett.* 9 (4) (2017) 39.
- J. Zhang, H. Luo, W. Xie, X. Lin, X. Hou, J. Zhou, S. Huang, W. Ou-Yang, Z. Sun, X. Chen, Efficient and ultraviolet durable planar perovskite solar cells via ferrocenecarboxylic acid modified nickel oxide hole transport layer, *Nanoscale* 10 (12) (2018) 5617–5625.
- J. Wang, X. Jia, J. Zhou, L. Pan, S. Huang, X. Chen, Improved performance of polymer solar cells by thermal evaporation of AgAl alloy nanostructures into the hole-transport layer, *ACS Appl. Mater. Interfaces* 8 (39) (2016) 26098–26104.
- M. Yao, P. Shen, Y. Liu, B. Chen, W. Guo, S. Ruan, L. Shen, Performance improvement of polymer solar cells by surface-energy-induced dual plasmon resonance, *ACS Appl. Mater. Interfaces* 8 (9) (2016) 6183–6189.
- M.D. Brown, T. Suteewong, R.S. Kumar, V. D'Innocenzo, A. Petrozza, M.M. Lee, U. Wiesner, H.J. Snaith, Plasmonic dye-sensitized solar cells using core-shell metal-insulator nanoparticles, *Nano Letters* 11 (2) (2011) 438–445.
- I.K. Ding, J. Zhu, W. Cai, S.-J. Moon, N. Cai, P. Wang, S.M. Zakeeruddin, M. Grätzel, M.L. Brongersma, Y. Cui, M.D. McGehee, Plasmonic dye-sensitized solar cells, *Advanced Energy Materials* 1 (1) (2011) 52–57.
- A.E. Shalan, T. Oshikiri, H. Sawayanagi, K. Nakamura, K. Ueno, Q. Sun, H.-P. Wu, E.W.-G. Diao, H. Misawa, Versatile plasmonic-effects at the interface of inverted perovskite solar cells, *Nanoscale* 9 (3) (2017) 1229–1236.
- Q. Luo, C. Zhang, X. Deng, H. Zhu, Z. Li, Z. Wang, X. Chen, S. Huang, Plasmonic effects of metallic nanoparticles on enhancing performance of perovskite solar cells, *ACS Appl. Mater. Interfaces* 9 (40) (2017) 34821–34832.
- C. Zhang, Q. Luo, J. Shi, L. Yue, Z. Wang, X. Chen, S. Huang, Efficient perovskite solar cells by combination use of Au nanoparticles and insulating metal oxide, *Nanoscale* 9 (8) (2017) 2852–2864.
- D. Thrithamarassery Gangadharan, Z. Xu, Y. Liu, R. Izquierdo, D. Ma, Recent advances in plasmon-enhanced promising third-generation solar cells, *Nanophotonics* 6 (1) (2017) 153–175.
- X. Liu, J. Iocozzia, Y. Wang, X. Cui, Y. Chen, S. Zhao, Z. Li, Z. Lin, Noble metal-metal oxide nanohybrids with tailored nanostructures for efficient solar energy conversion, photocatalysis and environmental remediation, *Energy Environ. Sci.* 10 (2) (2017) 402–434.
- G. Kakavelakis, K. Petridis, E. Kymakis, Recent advances in plasmonic metal and rare-earth-element upconversion nanoparticle doped perovskite solar cells, *J.*

- Mater. Chem. 5 (41) (2017) 21604–21624.
- [23] N. Fu, Z.Y. Bao, Y.-L. Zhang, G. Zhang, S. Ke, P. Lin, J. Dai, H. Huang, D.Y. Lei, Panchromatic thin perovskite solar cells with broadband plasmonic absorption enhancement and efficient light scattering management by Au@Ag core-shell nanocuboids, *Nanomater. Energy* 41 (2017) 654–664.
- [24] R.T. Ginting, S. Kaur, D.K. Lim, J.M. Kim, J.H. Lee, S.H. Lee, J.W. Kang, Plasmonic effect of gold nanostars in highly efficient organic and perovskite solar cells, *ACS Appl. Mater. Interfaces* 9 (41) (2017) 36111–36118.
- [25] P. Chen, Z. Xiong, X. Wu, M. Shao, Y. Meng, Z.H. Xiong, C. Gao, Nearly 100% efficiency enhancement of CH₃NH₃PbBr₃ perovskite light-emitting diodes by utilizing plasmonic Au nanoparticles, *J. Phys. Chem. Lett.* 8 (17) (2017) 3961–3969.
- [26] X. Chen, C. Zhao, L. Rothberg, M.-K. Ng, Plasmon enhancement of bulk heterojunction organic photovoltaic devices by electrode modification, *Appl. Phys. Lett.* 93 (12) (2008) 3021–3024.
- [27] L. Lu, Z. Luo, T. Xu, L. Yu, Cooperative plasmonic effect of Ag and Au nanoparticles on enhancing performance of polymer solar cells, *Nano Letters* 13 (1) (2013) 59–64.
- [28] B. Luk'yanchuk, N.I. Zheludev, S.A. Maier, N.J. Halas, P. Nordlander, H. Giessen, C.T. Chong, The Fano resonance in plasmonic nanostructures and metamaterials, *Nat. Mater.* 9 (9) (2010) 707–715.
- [29] A.E. Miroshnichenko, S. Flach, Y.S. Kivshar, Fano resonances in nanoscale structures, *Rev. Mod. Phys.* 82 (3) (2010) 2257–2298.
- [30] M. Yao, P. Shen, Y. Liu, B. Chen, W. Guo, S. Ruan, L. Shen, Performance improvement of polymer solar cells by surface-energy-induced dual plasmon resonance, *ACS Appl. Mater. Interfaces* 8 (9) (2016) 6183–6189.
- [31] M. Yao, X. Jia, Y. Liu, W. Guo, L. Shen, S. Ruan, Surface plasmon resonance enhanced polymer solar cells by thermally evaporating Au into buffer layer, *ACS Appl. Mater. Interfaces* 7 (33) (2015) 18866–18871.
- [32] J.R. Manders, S.W. Tsang, M.J. Hartel, T.H. Lai, S. Chen, C.M. Amb, J.R. Reynolds, F. So, Solution-Processed nickel oxide hole transport layers in high efficiency polymer photovoltaic cells, *Adv. Funct. Mater.* 23 (23) (2013) 2993–3001.
- [33] Z. Lu, X. Chen, J. Zhou, Z. Jiang, S. Huang, F. Zhu, X. Piao, Z. Sun, Performance enhancement in inverted polymer solar cells incorporating ultrathin Au and LiF modified ZnO electron transporting interlayer, *Org. Electron.* 17 (2015) 364–370.
- [34] W. Zhang, M. Saliba, S.D. Stranks, Y. Sun, X. Shi, U. Wiesner, H.J. Snaith, Enhancement of perovskite-based solar cells employing core-shell metal nanoparticles, *Nano Letters* 13 (9) (2013) 4505–4510.
- [35] V.M. Shalaev, S. Kawata, *Nanophotonics with Surface Plasmons*, Elsevier, 2007, p. 53.
- [36] H.J. Snaith, A. Abate, J.M. Ball, G.E. Eperon, T. Leijtens, N.K. Noel, S.D. Stranks, J.T. Wang, K. Wojciechowski, W. Zhang, Anomalous hysteresis in perovskite solar cells, *J. Phys. Chem. Lett.* 5 (9) (2014) 1511–1515.
- [37] Y. Bai, H. Chen, S. Xiao, Q. Xue, T. Zhang, Z. Zhu, Q. Li, C. Hu, Y. Yang, Z. Hu, F. Huang, K.S. Wong, H.-L. Yip, S. Yang, Effects of a molecular monolayer modification of NiO nanocrystal layer surfaces on perovskite crystallization and interface contact toward faster hole extraction and higher photovoltaic performance, *Adv. Funct. Mater.* 26 (17) (2016) 2950–2958.
- [38] Z. Jiang, X. Chen, X. Lin, X. Jia, J. Wang, L. Pan, S. Huang, F. Zhu, Z. Sun, Amazing stable open-circuit voltage in perovskite solar cells using AgAl alloy electrode, *Sol. Energy Mater. Sol. Cell.* 146 (2016) 35–43.
- [39] R.T. Ginting, E.-S. Jung, M.-K. Jeon, W.-Y. Jin, M. Song, J.-W. Kang, Low-temperature operation of perovskite solar cells: with efficiency improvement and hysteresis-less, *Nanomater. Energy* 27 (2016) 569–576.
- [40] M.F. Xu, X.Z. Zhu, X.B. Shi, J. Liang, Y. Jin, Z.K. Wang, L.S. Liao, Plasmon resonance enhanced optical absorption in inverted polymer/fullerene solar cells with metal nanoparticle-doped solution-processable TiO₂ layer, *ACS Appl. Mater. Interfaces* 5 (8) (2013) 2935–2942.
- [41] X. Chen, F. Zhu, Z. Lu, J. Yang, S. Huang, Z. Sun, Efficiency enhancement of inverted polymer solar cells using ionic liquid-functionalized carbon nanoparticles-modified ZnO as electron selective layer, *Nano-micro Lett.* 6 (1) (2013) 24–29.
- [42] G. Garcia-Belmonte, A. Munar, E.M. Barea, J. Bisquert, I. Ugarte, R. Pacios, Charge Carrier mobility and lifetime of organic bulk heterojunctions analyzed by impedance spectroscopy, *Org. Electron.* 9 (5) (2008) 847–851.